We are IntechOpen, the world's leading publisher of Open Access books Built by scientists, for scientists

4,800
Open access books available

122,000
International authors and editors

135M
Downloads

Our authors are among the

154
Countries delivered to

TOP 1%
most cited scientists

12.2%
Contributors from top 500 universities

CLARIVATE ANALYTICS BOOK CITATION INDEX INDEXED

WEB OF SCIENCE™

Selection of our books indexed in the Book Citation Index in Web of Science™ Core Collection (BKCI)

Interested in publishing with us?
Contact book.department@intechopen.com

Numbers displayed above are based on latest data collected.
For more information visit www.intechopen.com

Chapter

Whispering Gallery Modes for Accurate Characterization of Optical Fibers' Parameters

Martina Delgado-Pinar, Xavier Roselló-Mechó, Emmanuel Rivera-Pérez, Antonio Díez, José Luis Cruz and Miguel V. Andrés

Abstract

Whispering gallery modes (WGMs) are surface modes that propagate azimuthally around resonators with rotational symmetry (toroidal, spherical, or, as in our case, cylindrical shaped, since the optical fiber itself plays the role of the microresonator). These modes are resonant in optical wavelength, and the spectral position of the resonances depends on the radius and the refractive index of the microresonator material. Due to the high-quality factor of the resonances (as high as 10^7 in cylindrical microresonators), they allow measuring different parameters with high sensitivities and very low detection limits. Here, we report the use of WGMs to characterize the properties of the material that forms the microresonator. In particular, we highlight the use of this technique to measure temperature profiles along conventional and special fibers (such as photosensitive or doped fibers), elasto-optic coefficients, and UV-induced absorption loss coefficients of different photosensitive fibers. These parameters of the fibers set the optical response of fiber-based components and may change when the device is in use in an optical system; thus, this technique allows an accurate characterization of the devices and leads to proper designs of components with specific optical responses.

Keywords: whispering gallery modes, surface modes, microresonators, optical fibers, fiber Bragg gratings, elasto-optic effect, thermo-optic effect

1. Introduction

Whispering gallery modes are surface modes that propagate azimuthally around resonators with rotational symmetry, generally a dielectric. This phenomenon was first described by Lord Rayleigh in the nineteenth century, when studying the propagation of acoustic waves in interfaces with a curvature [1]. St. Paul's Cathedral (London, UK), the Temple of Heaven (Beijing, China), the Pantheon (Rome, Italy), the Tomb of Agamemnon (Mycenae, Greece), and the Whispering Gallery in the Alhambra (Granada, Spain) are examples of architectonical structures that support acoustic modes which propagate guided by the surface of the walls. It was at the beginning of the twentieth century when the study of this guiding mechanism was extended to the electromagnetic waves, since Mie developed his theory for the

plane electromagnetic waves dispersed by spheres with diameters of the same size as the optical wavelength [2]. Shortly after, Debye stablished the equations for the optical resonances of dielectric and metallic spheres based on Mie's dispersion theory [3]. The detailed study of the mathematical equations of WGMs was performed by Richtmyer [4] and Stratton [5], who predicted high-quality factors Q for these resonances and led to its implementation in different technologies based on microwave and acoustic waves. In the microscopic world, light can be guided by the same mechanism, when the resonator has dimensions of tens to hundreds of microns, and the wavelength of the light is in the visible-infrared range. In 1989, Braginsky et al. set the beginning of the optical WGMs when reporting the technique to excite optical modes in microresonators with spherical shape [6]. Since then, many researchers have studied the propagation of WGMs in structures with different symmetries [7] and have reported efficient methods based on microtapers to excite these modes in the optical range [8].

Due to the intrinsic low losses, WGMs show very high Q factors. For example, they can achieve values of 10^{10} in spheres [9], 10^8 in silicon microtoroids [10], or 10^6–10^7 in cylindrical microresonators [11]. At the resonance, the light guided by a WGM is recirculated in the microresonator many times, which provides a mechanism for decreasing the detection limit of the sensors based on them. This enhanced detection limit has been demonstrated to be low enough to measure a single molecule on the surface of a microtoroid [12].

WGM resonances shift in wavelength as the refractive index of the external medium changes. The sensitivity of WGMs as a function of these variations is significant: when considering a silica-cylindrical microresonator of 125 μm in diameter, immersed in water ($n = 1.33$), the calculated shift in wavelength of the resonance is 77 nm/RIU. For a typical resonance width of 0.5 pm, this leads to a detection limit of 6×10^{-6} RIU. It is worth to note that the light guided by WGMs is mainly confined in the microresonator. Thus, their sensitivity to variations of the material refractive index will be even higher. For example, it can achieve values as high as 1.1 μm/RIU when considering variations of the refractive index of the silica. In this example, the detection limit of the WGM decreases down to 4×10^{-7} RIU. In this chapter, we will report the use of WGMs in silica, cylindrical microresonators (an optical fiber) to measure and characterize the properties of the microresonator itself. There are a number of parameters, such as temperature or strain, which modify the refractive index of the material. Thus, this technique allows measuring with accuracy variations of temperature in doped optical fibers, in optical devices as fiber Bragg gratings (FBG), the elasto-optic coefficients of conventional silica fibers, and the absorption coefficient of photosensitive optical fibers, for example. We will report here the fundamentals of the technique, as well as the experimental results we obtained for these experiments.

2. Fundamentals

The guiding mechanism of WGMs in the azimuthal direction of a microresonator (MR) is total internal reflection, just as in the case of axial propagation in a conventional waveguide; see **Figure 1a**. Resonance occurs when the guided wave travels along the perimeter of the MR, and it drives itself coherently by returning in phase after every revolution. In its way, the wave follows continuously the surface of the MR, and the optical path in a circumnavigation must be equal to an integer multiple of the optical wavelength, λ. When this condition is fulfilled, resonances appear, and a series of discrete modes at specific wavelengths will show up. The resonant condition can be written as [13]

$$\lambda_R = \frac{2\pi a \cdot n_{\text{eff}}}{m} \tag{1}$$

where λ_R is the resonant wavelength, a is the radius of the MR, n_{eff} is the effective index of the WGM, and m is the azimuthal order of the mode (i.e., the number of wavelengths in the perimeter of the MR). The effective indices of the different modes are calculated, as usual, by solving Maxwell's equations and applying the proper boundary conditions [5]. In our case, we will deal with cylindrical, dielectric MRs with translational symmetry in the axial direction (see **Figure 1b**). Two zones can be identified, regions I (of radius a) and II (which extends to the infinite), with refractive indices n_1 and n_2, respectively, with $n_1 > n_2$. The magnetic permeability of the material and of the external medium is equal to that of the vacuum, μ_0, and both media are homogeneous although, in general, they present an anisotropy in the dielectric permittivity. In the axial direction, we will consider a refractive index of the material n_{1z} which is different to the refractive index in the transversal directions, n_{1t} (see Eq. (2) for the expression of the tensor of the refractive index):

$$n_2 = \begin{pmatrix} n_{1t} & 0 & 0 \\ 0 & n_{1t} & 0 \\ 0 & 0 & n_{1z} \end{pmatrix} \tag{2}$$

We do not intend to give a full description of the solution of this problem, which can be found in [14], but we will summarize the main equations and features of WGMs.

If we solve Maxwell's equations with this uniaxial tensor, the modes split in two series of family modes that, analogously to the case of axial waveguides, are denoted as TE-WGMs, which show a transversal electric field ($e_z = 0$), and TM-WGMs, with transversal magnetic field ($h_z = 0$). Each series of modes is ruled by a transcendental equation that must be solved: Eq. (3) for TM modes and Eq. (4) for TE modes. The solutions consist on a series of discrete wavelengths, which correspond to the different radial orders l of each m^{th} value. With these values, it is possible to calculate the effective indices of each WGM resonance using Eq. (1):

$$n_{1z}\frac{J_{m'}(k_0 n_{1z} a)}{J_m(k_0 n_{1z} a)} = n_2 \frac{H_m^{(2)'}(k_0 n_2 a)}{H_m^{(2)}(k_0 n_2 a)} \tag{3}$$

$$\frac{1}{n_{1t}}\frac{J_{m'}(k_0 n_{1t} a)}{J_m(k_0 n_{1t} a)} = \frac{1}{n_2}\frac{H_m^{(2)'}(k_0 n_2 a)}{H_m^{(2)}(k_0 n_2 a)} \tag{4}$$

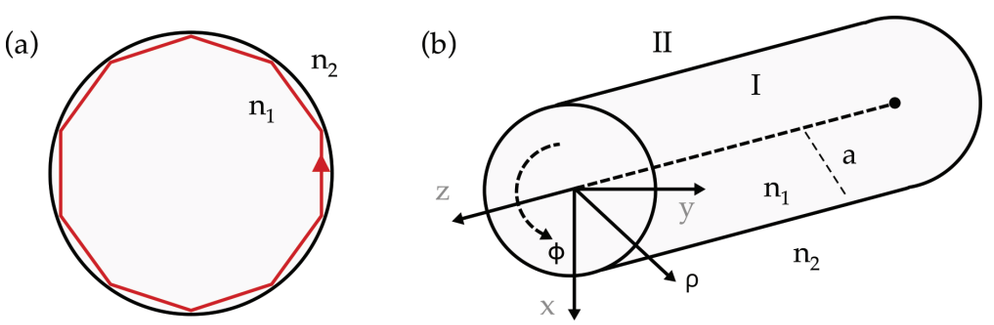

Figure 1.
(a) Scheme of the WGM propagating azimuthally in the MR. (b) Cylindrical system of coordinates which shows the two regions considered in the problem.

In Eqs. (3) and (4), k_0 is the wavenumber in vacuum, $k_0 = 2\pi/\lambda$, J_m is the Bessel function of order m and J'_m is its first derivative, $H_m^{(2)}$ is the second class Hankel function of order m, and $H_m^{(2)'}$ is its first derivative. We have considered that the external medium does not present any anisotropy (in our case, it will be air).

By following this procedure, it is possible to calculate the dispersion curves of several WGMs propagating in a cylindrical, silica MR of 125 μm diameter (the parameters of conventional optical fibers). Sellmeier dispersion of the silica was taken into account for the refractive index of the material. It is worth to note that the dispersion curves are not truly a curve, but a series of discrete solutions that have a particular radial order l and azimuthal order m. For a standard optical fiber and 1550 nm optical wavelength, the azimuthal orders will be relatively high ($m \sim 300$). **Figure 2** shows the calculations of the resonant wavelengths for the first radial orders, as a function of the azimuthal order m for the TM polarization. The curves for the TE polarization follow the same trend, but the values of the resonant wavelengths are slightly different. By using Eq. (1), it is possible to relate the resonant wavelength with the effective index of the WGM resonance. For the azimuthal order $m = 360$ and the first radial order, $l = 1$, the resonant wavelengths and the effective indices of both polarization families are $\lambda_R^{\mathrm{TM}} = 1508.25$ nm, $n_{\mathrm{eff}}^{\mathrm{TM}} = 1.3826$ and $\lambda_R^{\mathrm{TE}} = 1505.39$ nm, $n_{\mathrm{eff}}^{\mathrm{TE}} = 1.3800$. Thus, the resonances for each polarization are not overlapped in wavelength.

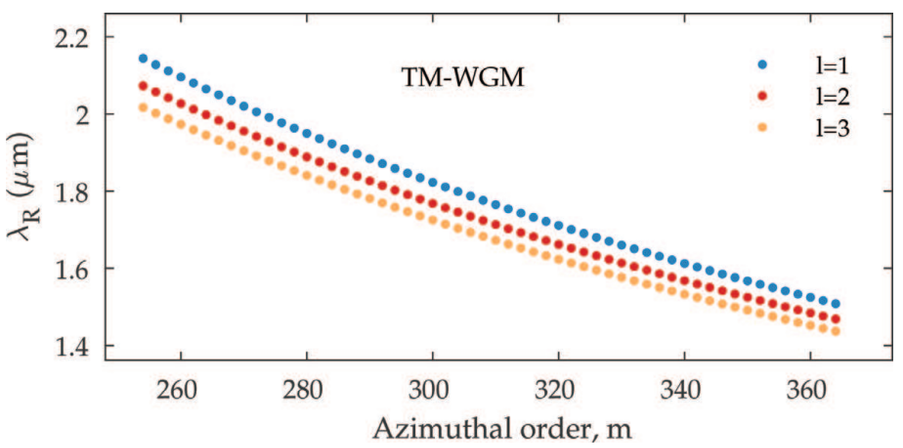

Figure 2.
Resonant wavelength of WGMs with azimuthal orders from 250 to 370. Only a selection of the solutions to highlight their discrete nature is shown.

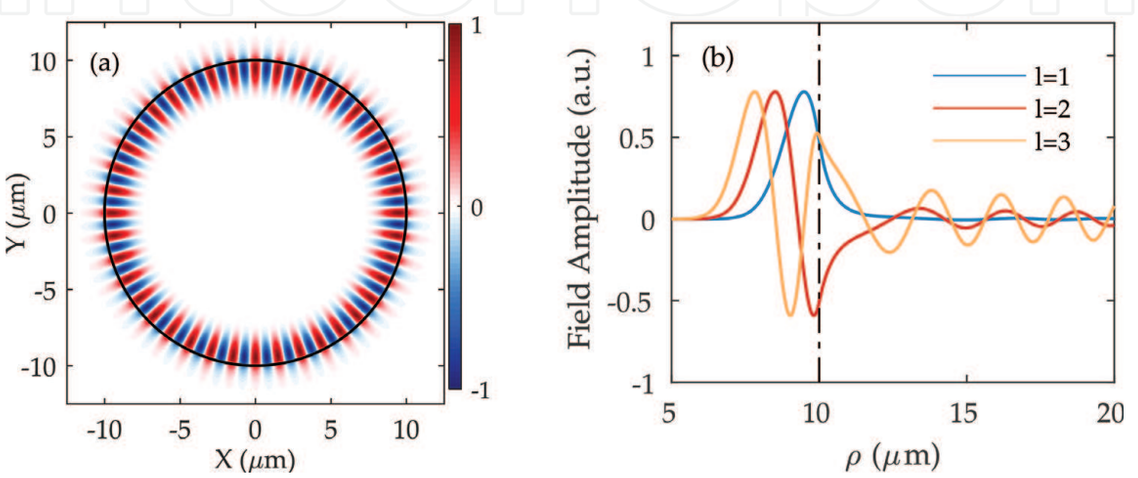

Figure 3.
(a) Optical field of a $m = 40$ and $l = 1$ WGM in a silica, cylindrical MR. (b) Field amplitude of the WGM as a function of the radial coordinate, for $m = 40$ and $l = 1, 2, 3$.

Regarding the distribution of the fields, **Figure 3a** shows the amplitude of the electric field of the first radial order TM-WGM, propagating in a cylindrical, silica MR of 10 μm diameter (the order m of the mode is 40; a low-order mode was considered in order to show the details of the field). As it can be observed, the field is well confined within the MR material (although its evanescent field is high enough to enable the use of these modes for sensing). As the azimuthal order of the WGM gets higher, the field will be more localized near the interface between the MR and the external medium. Also, it should be noted that, as the radial order of the WGM increases, the evanescent tail in the outer medium is larger; thus the quality factor of the correspondent resonance will be poorer. **Figure 3b** shows the field amplitude along the radial coordinate of the MR. As it can be observed, the optical power is localized in the outer region of the MR, near the interface, and shows a low-evanescent field in the outer medium, especially for the $l = 1$ mode.

3. Experimental setup

The general setup used in the experiments is shown in **Figure 4a**. The light source is a tunable diode, linearly polarized laser (TDL) with a narrow linewidth (<300 kHz). The tuning range covers from 1515 to 1545 nm. The laser integrated a piezoelectric-based fine frequency tuning facility that allows continuous scanning of the emitted signal around a given wavelength, with subpicometer resolution. A polarization controller (PC) after the laser allows rotating the polarization of the light, and, as a consequence, it allows exciting TE- and TM-WGMs separately. The optical signal is then launched through an optical circulator, which enables measuring the WGM resonances in reflection by means of a photodetector (PD).

The MR will consist on a section of the bare optical fiber under test (FUT). Depending on the experiment, it will be a conventional telecom fiber, a rare-earth doped fiber, a photosensitive fiber, or a fiber where a grating has been previously inscribed. It is carefully cleaned and mounted on a three-axis flexure stage. WGMs are excited around the FUT by using the evanescent optical field of an auxiliary microtaper with a waist of 1–2 μm in diameter and a few millimeters in length. This is not the only method that allows exciting WGMs in MRs: for example, one of the first techniques consisted on using a prism to excite the resonances in a spherical MR [15], but the efficiency was very poor. More recently, a fused-tapered fiber tip fabricated using a conventional fiber splicer was demonstrated to be capable of exciting WGMs in a cylindrical MR [16]. However, the highest efficiencies are achieved by using microtapers, with coupling efficiencies higher than 99% [8]. These microtapers are fabricated by the fuse-and-pull technique from conventional

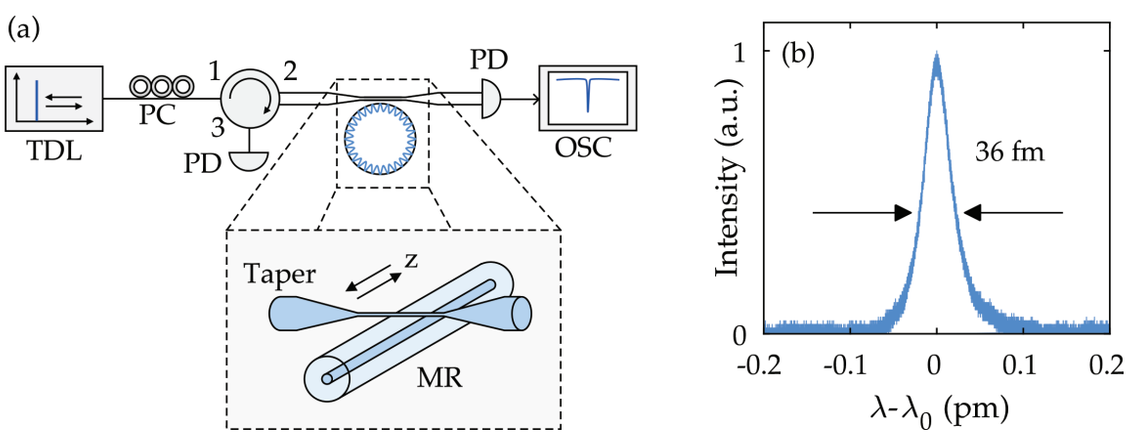

Figure 4.
(a) Scheme of the experimental setup. (b) Typical reflection spectrum of a WGM.

telecom fiber [17]. The microtaper and the MR are placed perpendicularly (see in the inset **Figure 4a**). Since the optical field of the WGMs is not axially localized (its extension is around 200 μm in length [7]), this setup allows exciting the WGM at different positions along the MR: by sweeping the microtaper along the MR, it is possible to detect variations of the parameters of the MR in the axial direction by measuring the shift of the resonances—radius [13, 18], temperature, or strain. Variations can be characterized along several centimeters of the MR.

The transmission of the taper was measured using a photodetector, and the signal was registered by an oscilloscope synchronized with the TDL. A typical transmission trace consists on a signal that will present a series of notches at the resonant wavelengths. For MRs of 125 μm in diameter, the free spectral range between two consecutive azimuthal orders m is $\sim$ 4 nm at 1550 nm, and it is the same for both polarizations. **Figure 4b** shows the reflection spectrum of a resonance in an optical fiber ($a = 62.5\ \mu m$): its linewidth is 36 fm, which corresponds to a Q-loaded factor of 4×10^7.

As it was mentioned before, the position of the resonances will depend on the value of the refractive index of the material. In the next sections, we will study the characterization of different fibers and fiber components by means of the measurement of the shift of WGM resonances as the effective index of the MR is modified.

4. Measurement of temperature profiles in doped fibers and fiber gratings

When a silica fiber is heated up, two effects occur. First, the expansion of the fiber leads to a change of the diameter. Second, the thermo-optic effect induces a change in the refractive index of the material due to a variation of temperature. This variation modifies the spectral position of the WGM. From Eq. (1) it is possible to evaluate the shift of the resonant wavelength, $\Delta\lambda_R$, of a WGM due to a variation of temperature, ΔT:

$$\frac{\Delta\lambda_R}{\lambda_R} = \left(\frac{1}{\mathrm{a}}\frac{d\mathrm{a}}{dT} + \frac{1}{n_{\mathrm{eff}}}\frac{dn_{\mathrm{eff}}}{dT}\right) \cdot \Delta T \tag{5}$$

In the case of optical fibers as MRs, it is a good approximation to assume that the thermo-optic coefficient (i.e., the second term in Eq. (5)) can be replaced by that of the pure silica, since the optical field of the WGMs is mainly localized in the fiber cladding (see **Figure 3**). The high sensitivity of WGMs to variations of temperature has been demonstrated for different geometries of the MR, such as microspheres [19, 20] or cylinders [21]. Moreover, the propagation of an optical signal of moderate power ($\sim$ 1 W or higher) in a fiber generally induces a variation of temperature of the material. Due to the variation of temperature, the optical response of the fibers, or fiber components, may change when they are in operation. Thus, a detailed characterization of this effect is of interest to design properly the fiber-based optical systems. The use of WGMs allows achieving a very low detection limit: Rivera et al. claimed a detection limit of two thousandths of degree [21].

Here, we will present the characterization of temperature variations in two different examples: (i) rare-earth doped active fibers and (ii) fiber gratings inscribed in commercial photosensitive fibers.

4.1 Measurement of temperature in rare-earth doped fibers

Heating of rare-earth doped fibers can be an issue in fiber-based lasers and amplifiers. For example, thermal effects can be a limit to the maximum output

power that these systems can provide [22]. Another example is the shift in wavelength observed in distributed Bragg reflectors (DBR) and distributed feedback (DFB) lasers due to a pump-induced increment of temperature [23]. The heat is due to the non-radiative processes related to the electronic relaxation of some dopants: for example, this effect is less important in ytterbium-doped fibers, while Er/Yb-codoped and erbium-doped fibers exhibited a high increase of temperature with pump, due to its specific electronic-level system [24]. Thus, it is an intrinsic characteristic of the doped fibers that one needs to evaluate in order to design the proper optical system.

In the experiments presented here, several commercially available single-mode, core-pumped doped fibers from Fibercore were investigated. Specifically, the FUTs were three Er-doped fibers (DF-1500-F-980, M12-980/125, and I25-980/125), a Yb-doped fiber (DF-1100), and an Er/Yb-codoped fiber (DF-1500 Y). The values for absorption coefficients at the pump wavelength were 5.5 dB/m (DF-1500-F-980), 12 dB/m (M12-980/125), 21.9 dB/m (I25-980/125), 1000 dB/m (DF-1100), and 1700 dB/m (DF-1100). Short sections of $\sim$ 2 cm in length of each FUT were used as the MR where the WGMs were excited. The FUTs were pumped with a single-mode, fiber-pigtailed laser diode that emitted a maximum power of 380 mW at 976 nm. As the pump launched to the FUT was increased, the WGM resonance shifted toward longer wavelengths in all cases, as it was expected, since the thermo-optic and the thermal expansion coefficients of silica are both positives. As an example, **Figure 5** shows the shift in wavelength of a resonance as a function of the pump launched to the fiber DF-1500-F-980. In our experiments, we did not investigate in detail the temporal response of the phenomenon, which will be ruled by the mechanisms that convert the pump power to heat, the heat conduction in silica, and the transfer of heat to the air. Typically, it will be on the range of a few tens of microseconds [25].

At this point, several features of this technique must be clarified. First, it is worth to point out that the shift in wavelength is virtually independent of the particular resonance used for the measurements, that is, it does not depend on its radial and azimuthal order nor on its polarization. The sensitivity to thermal variations of different WGM resonances was theoretically calculated around 1.53 μm, taking into account both the thermal expansion of the fiber and the thermo-optic effect. The results showed that the difference in sensitivity between different resonances differs in less than 1/10000 per each ^oC of temperature increase. This simplifies the utility of this technique.

The second aspect to highlight is related to the fact that the dopants in the active fibers are located in their core, while WGMs are highly confined in the outer region of the cladding (see **Figure 3**). From the study of heat conduction in doped fibers

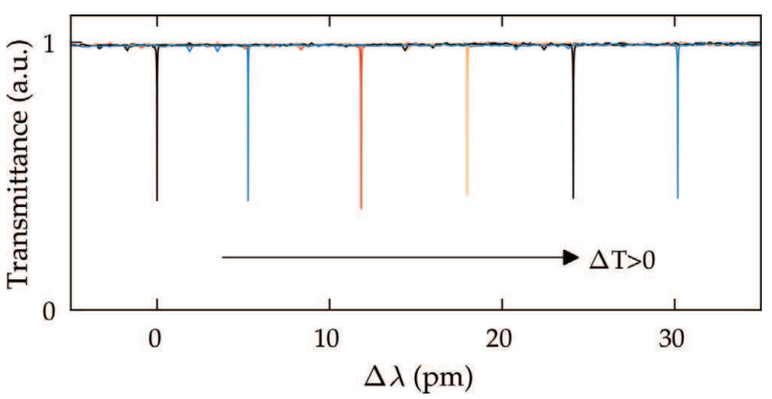

Figure 5.
Wavelength shift of the resonant wavelength as the pump power is increased. From left to right: pump power 0 mW, 40 mW, 110 mW, 180 mW, 270 mW, and 370 mW.

carried out by Davis et al. [25], it is possible to calculate that, at the steady state, the increase of temperature at the core of the fiber is just 1.5% larger than at the outer surface.

In order to calibrate the shift in wavelength of the WGM resonances with the heating, a FBG inscribed in the core of a doped fiber was used for comparison. The procedure is described in [21]. The WGM resonances shift at a rate of 8.2 pm/^oC. With this calibration, it is possible to correlate the shifts in wavelength with the increase of temperature in the core of the fiber. For the example shown in **Figure 5**, the maximum increment of temperature achieved for a pump of 370 mW was 3.7^oC.

Figure 6 summarizes the measurements performed for the different doped fibers. A similar trend can be observed in all the cases; the resonances shift fast in wavelength for low pump powers, and, beyond certain pump, heating tends to saturate. It can be observed that the Yb fiber DF 1100 shows a similar increase of temperature to those of the Er-doped fibers, although the concentration of the dopants in the Yb fiber is much larger (note the absorption coefficient around 975 nm). Also, the highest temperature increment corresponds to the Er/Yb-doped fiber (DF 1500 Y), despite that it shows a lower absorption coefficient than its equivalent Yb-doped fiber (DF 1100). These results are in accordance to the fact that the heating is related to the existence of non-radiative transitions for the relaxation of electrons in the active medium.

4.2 Measurement of temperature profiles in fiber components

As it was mentioned before, WGMs are axially localized: their extension along the fiber is $\sim 200\ \mu m$, typically, for a MR of 62.5 μm. Thus, this technique provides spatial resolution. The taper can be swept along the MR in order to characterize the parameters of the FUT point to point. This feature was used in order to characterize the temperature profile along fiber components [26].

The FBGs used in the experiments were written in germanium-silicate boron codoped, photosensitive fibers from Fibercore, using a doubled-argon UV laser and a uniform phase mask. The length of all the gratings was $\sim$ 10 mm. The WGMs were excited at different positions along the FBG, and, simultaneously, it was illuminated by optical signals of moderate powers, within or outside of the

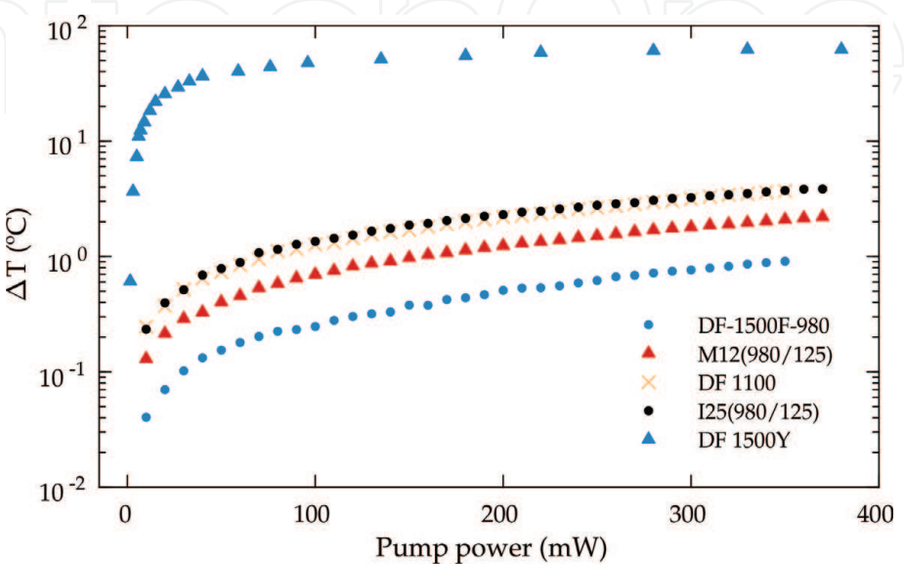

Figure 6.
Heating of the doped fibers as a function of pump power.

reflection band but in the vicinities of the Bragg wavelength. This illumination signal was provided by an amplified tunable laser (range, 1520–1560 nm) that provided up to 1 W of CW light.

As a preliminary experiment, a section of fiber Fibercore PS980 was uniformly irradiated (i.e., there was no grating inscribed). The length was 5 mm, and the UV fluence power used in the irradiation was 150 J/mm^2. The wavelength shift of the resonances was measured as the MR was illuminated with a 1550 nm optical signal, compared to the original position of the resonances, with no illumination along the FUT. **Figure 7a** shows the results. The data show a clear difference between the irradiated length ($z < 3$ mm) and the non-irradiated length ($z > 3$ mm). A temperature gradient in an intermediate region due to the heat conduction in silica and the transfer of heat to the air can be observed. It should be noted that this section is far larger than the length of the focused UV beam ($\sim 700\ \mu m$); thus, the beam size is not the cause of this transition length. In the irradiated section, the temperature increases at a rate higher than 10 $^oC/W$, for this sample, while the pristine fiber heats up at a rate lower than 1 $^oC/W$. The increment of temperature was linear with power in the available power range. This experiment avails that this technique allows characterizing the variations of temperature along the components with a resolution of tenths of a millimeter. This feature is useful when one needs to detect, evaluate, and correct smooth undesired non-homogeneities that may occur during the fabrication of FBG and LPG, which are usually short components. As an example, **Figure 7b** shows the measurement of the temperature profile of a section of an irradiated fiber (length, 5 mm) that suffered from some misalignment during the UV irradiation process. For this sample, a variation of 4 ^oC is measured in such a short irradiated length.

The temperature profile along a FBG with strong reflectivity was measured using this technique. The FBG had a reflectivity higher than 99.9%; the Bragg wavelength was 1556 nm, its length was 12 mm, and it was fabricated in PS1250 fiber (Fibercore). First, the illumination signal was tuned well outside the reflection band, at 1540 nm; in this case, there is no reflection of the optical signal; it just propagates through the FBG. The power launched to the MR was 800 mW. Curve (i) in **Figure 8** shows the obtained results. As expected, a similar result to the case shown in **Figure 7a** was obtained: the heating over the length of the FBG was fairly constant, $\sim 5.5\ ^oC$. It should be noted that the axial resolution of the technique will be larger than the grating period. Then, the average increment of temperature should be similar to that introduced in the case of the uniformly irradiated fiber, for

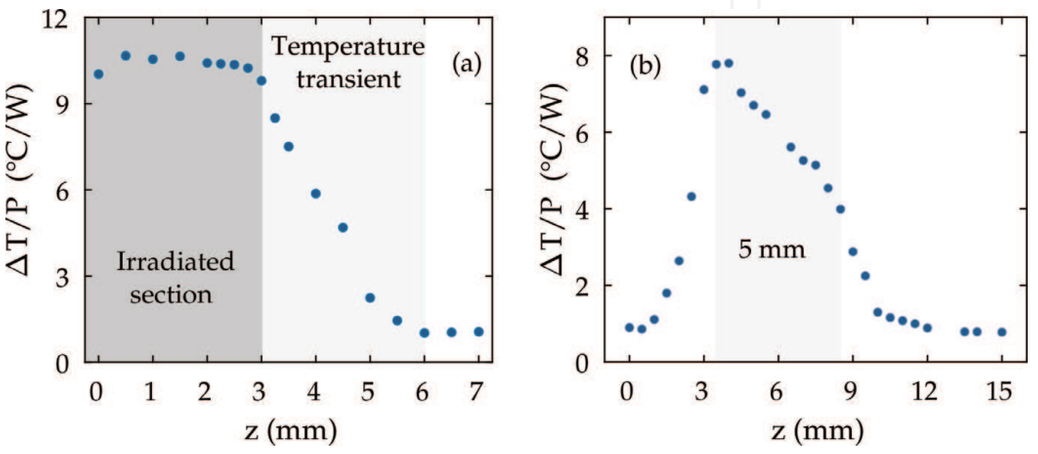

Figure 7.
Temperature profile of irradiated FUTs, (a) uniformly and (b) nonuniformly.

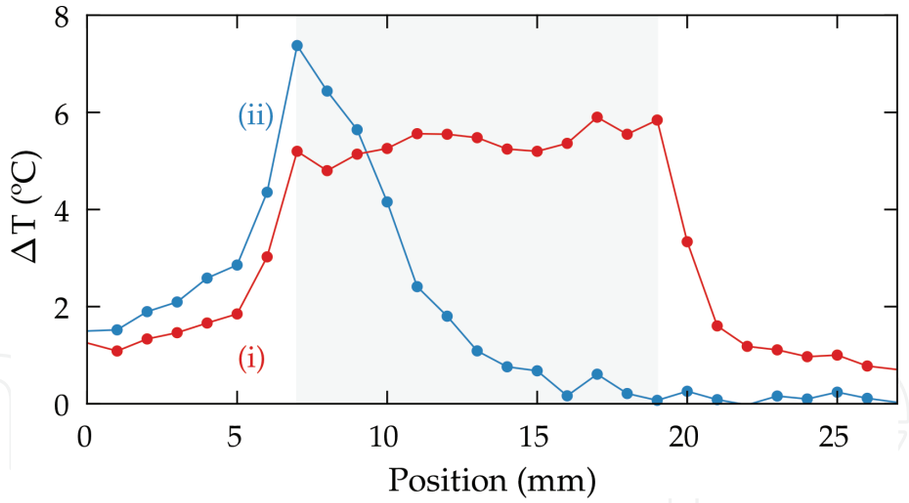

Figure 8.
Temperature profile of a FBG illuminated (i) outside and (ii) within the reflexion band.

the same UV fluence and fiber characteristics. Two transition zones were clearly observed at both ends of the grating.

Finally, the temperature profile was measured when the optical signal was tuned to the Bragg wavelength (power, 1 W) (see curve (ii) in **Figure 8**). In this case, one should take into account that the UV irradiation is constant over its length, and the gradient temperature is due to the fact that the optical signal is reflected as it penetrates into the grating. A sharp increment of temperature at the beginning of the grating, at the extreme that is illuminated, can be observed. The maximum is located at the vicinities of the point where the FBG begins. The decay of temperature extends over a length of ~ 5 mm, which is shorter than the length of the fiber itself (12 mm). This is consistent with the high reflectivity of this FBG. Moreover it should be noted that, at the beginning of the curve, that is, $z = 0 - 3$ mm, the temperature increase is $\sim 2\ ^oC$, that is, roughly twice the value obtained for a pristine fiber. On the contrary, in the section after the grating (and even at the last millimeters of the FBG), the increment of temperature is below the detection limit of the technique. The origin of this asymmetry is the reflection of the optical signal: the amount of light that reaches the last millimeters of the FBG is very small. This technique, then, provides information about the effective length of gratings of different reflectivity, information that could be relevant for the design of optical systems that require of short cavities, or cavities that require of a very precise length, as in the case of mode-locked fiber lasers.

5. Measurement of absorption coefficients in photosensitive fibers

In the previous section, the gradient of temperature induced in fiber-optic components by means of an illumination signal has been characterized and discussed. It has been shown that there is a difference in temperature between the sections that have been irradiated with UV light compared to the pristine fibers. It is well known that the UV irradiation induces a change in the index of photosensitive fibers, which is employed to fabricate FBGs and LPGs. According to Kramers-Kronig relations, the change in the refractive index is associated with a variation of the absorption coefficient. In addition, the exposure of the fiber to the levels of UV light usually employed in the grating fabrication induces mechanical deformations in the fiber [27]. This leads to an increase of the loss due to scattering. Thus, when a

fiber is UV irradiated, its loss, α, increases due to two causes: absorption that will be quantified by α^{abs} and scattering, α^{scat}.

The increase of α introduced by UV irradiation has been measured before [28], since this is a parameter of interest to optimize the fabrication of FBGs, especially in the case of long or superimposed gratings with many reflection bands [29, 30]. This measurement provides information about an averaged value of the attenuation loss along the irradiated section, which includes both the absorption and the scattering contributions. The technique based on the measurement of the shift of WGM resonances will only measure the absorption coefficient; thus, by combining the two types of measurements, it is possible to evaluate both contributions separately.

Different types of photosensitive fibers were studied [11]: (i) Fibercore PS980, (ii) Fibercore PS1250, (iii) Fibercore SM1500, and (iv) Corning SMF28; this fiber was hydrogenated for 15 days (pressure: 30 bar) to increase its photosensitivity. The setup used in the experiments was the same than in the previous experiments shown in this chapter. In this case, the FUTs were short sections of the different fibers, which were exposed to a UV fluence of 150 J/mm^2. Similar temperature profiles to that shown in **Figure 7a** were obtained for all of them, but with different temperature increments, since the photosensitivity was also different for each of them.

The different increases of temperature between the irradiated fiber and the pristine fiber will provide us information to quantify the variation in the α^{abs} due to UV irradiation. It will be assumed that the heating over the transversal section of the fiber, at a given axial position, is set by the absorption coefficient, α^{abs}. According to the analysis reported by Davis et al. [25], the heating at the steady state, ΔT, will be given by

$$\frac{\Delta T}{P} = \frac{1}{2\pi a h}\alpha^{abs} \tag{6}$$

where h is the heat transfer coefficient (81.4 $W \cdot m^{-2} \cdot K^{-1}$ for a silica fiber). Then, the ratio of ΔT between two different points along the FUT, 1 and 2, is given by

$$\frac{\Delta T_2}{\Delta T_1} = \frac{\alpha_2^{abs}}{\alpha_1^{abs}} \tag{7}$$

Thus, with this analysis and the experimental data obtained from the measurement of the wavelength shift of WGM resonances in irradiated points (1) and pristine points (2) of the FUT, this ratio between the respective α^{abs} can be calculated.

Direct measurements of transmission loss variation as the fibers were irradiated were carried out for a PS980 fiber. First, the value of the loss of the pristine fiber was measured at 1550 nm by means of the cutback method: the obtained value was 120.0 ± 0.5 dB/km. Then, the UV laser was swept back and forth along a 5-cm-long section of the fiber, repeatedly. The full description of the procedure is described in [11]. **Figure 9a** shows the data obtained in this experiment. The final loss was 6.2 ± 0.4 dB/m; thus the ratio between the loss coefficients, α_2/α_1, increased 52 ± 3 times. Please remember that this loss coefficient includes both absorption and scattering contributions ($\alpha = \alpha^{abs} + \alpha^{scat}$).

The contribution to the loss by means of the absorption mechanism was measured using the WGM technique (see **Figure 9b**). In this case, a 1550 nm laser (maximum power, 1 W) was launched to the FUT, and the thermal shift of the

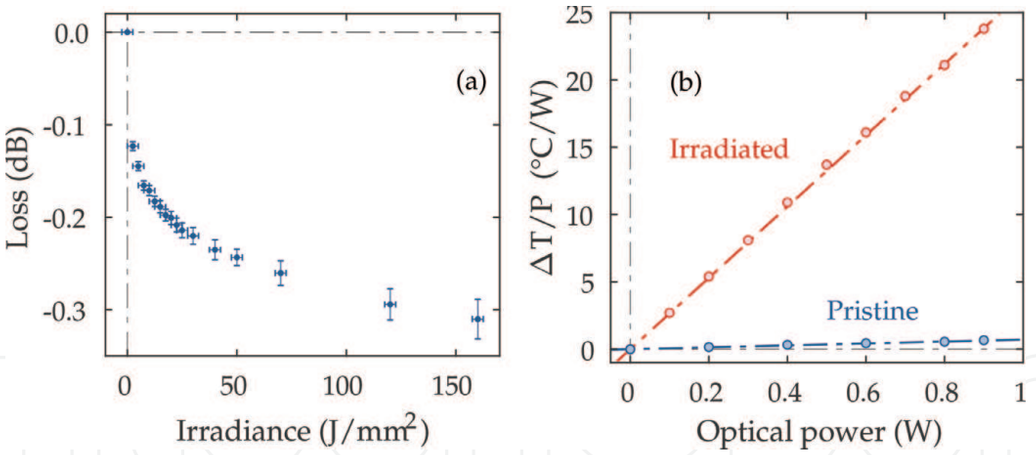

Figure 9.
(a) Direct measurement of the loss as the PS980 fiber is irradiated. (b) Heating of the PS980 fiber as a function of the illumination power.

	WGM technique			Direct measurements		
	$1-\alpha_2^{abs}/\alpha_1^{abs}$	$\Delta T/P\ (^oC/W)$		α_2/α_1	α (dB/km)	
		Irradiated	Pristine		Irradiated	Pristine
PS980	36.9 ± 0.7	26.48 ± 0.15	0.718 ± 0.014	52 ± 3	6200 ± 400	120 ± 2[3]
PS1250	40.1 ± 0.8	30.80 ± 0.17	0.768 ± 0.014	50 ± 3	6600 ± 400	131.1[4]
SM1500	>40[1]	1.20 ± 0.03	< 0.03[2]	190 ± 50	370 ± 90	1.95[4]
H_2-SMF28	28.8 ± 0.5	23.48 ± 0.13	0.815 ± 0.012	n/a[2]	5600 ± 400	n/a[1]

[1]*Nonavailable.*
[2]*Below detection limit.*
[3]*Cutback measurement.*
[4]*Nominal value.*

Table 1.
Measurement of thermal heating and loss coefficient of different fibers.

resonances was measured as the laser power was increased, at two different points, one within the irradiated section and one outside it. The data does not show any sign of saturation of the heating, at this range of power. The temperature of the irradiated section increased linearly, at a rate of $26.48 \pm 0.15\ ^oC/W$, and at $0.718 \pm 0.014\ ^oC/W$ in the pristine region. The ratio between these values, that is, the ratio $\alpha_2^{abs}/\alpha_1^{abs}$, is $36.9 \pm 0.7\ ^oC/W$.

This process was repeated for all the different fibers mentioned before: PS1250, SM1500, and hydrogenated SMF28, at 1550. **Table 1** includes the results from the measurements and the corresponding analysis: α_2/α_1 was obtained for each of them from the direct measurement of the loss, while $\alpha_2^{abs}/\alpha_1^{abs}$ was calculated from the technique based in WGMs.

The results, compiled in **Table 1**, allow establishing several conclusions of interest. First, as expected, the absorption coefficient is substantially increased due to the UV irradiation. As a consequence, even for signals of moderate powers, FBGs might experience shifts and chirps that should be taken into account [31]. Second, the results show that α_2/α_1 is systematically higher than $\alpha_2^{abs}/\alpha_1^{abs}$. Roselló-Mechó et al. analyzed the measurements to demonstrate that these results lead to the conclusion that scattering loss increases at a higher rate than absorption loss [11].

Finally, Eq. (6) can be used to calculate the absolute value of the absorption and scattering coefficients by taking into account the values of h and a for a silica

	α^{abs} (dB/km)		α^{scat} (dB/km)	
	Irradiated	**Pristine**	**Irradiated**	**Pristine**
PS980	3680 ± 20	99.7 ± 1.9	2500 ± 400	20 ± 3
PS1250	4280 ± 20	106.6 ± 1.9	2300 ± 400	24.5 ± 1.9
SM1500	167 ± 4	< 1.95[1]	200 ± 90	< 1.95[1]
H_2-SMF28	3260 ± 18	113.1 ± 1.7	2300 ± 400	n/a[2]

[1]*Nominal value.*
[2]*Nonavailable, hydrogenated fiber.*

Table 2.
Absorption and scattering contributions to the overall attenuation coefficient.

fiber [25] and the measurements of α. The results of the contributions are compiled in **Table 2**. Both contributions are in the same order of magnitude, but α^{scat} is smaller for three of the four FUTs. These values confirm that scattering loss increases faster than absorption loss.

Thus, by means of the combination of both techniques, it is possible to quantify the different contributions to the loss, even for short sections of fiber. This information might be useful, for example, in the design of novel-active doped fibers, since it is possible to evaluate if the doping technique increases the scattering loss unnecessarily, but not so much the absorption.

6. Measurement of Pockels coefficients in optical fibers

The elasto-optic effect consists on the variation in the refractive index generated by any strain applied to the fiber. The correspondent elasto-optic coefficients are usually determined by measuring the optical activity induced by a mechanical twist and the phase change induced by longitudinal strain [32, 33]. This technique relies on the use of the conventional axial modes propagating through the fiber. Since these modes are essentially transverse to the axis of the fiber [34], the anisotropy of the elasto-optic effect does not show up. On the contrary, WGMs have a significant longitudinal component; hence, their optical fields experience the anisotropy of the elasto-optic effect intrinsically. In the last years, researchers have demonstrated a number of fiber devices in which the longitudinal components of the electromagnetic modes are significant, such as microfibers [35] and microstructured optical fibers with a high air-filling fraction [36]. For these cases, the measurement and characterization of the anisotropy of the elasto-optic effect and its Pockels coefficients are of high interest. Roselló-Mechó et al. reported a technique based on the different wavelength shifts of TE- and TM-WGM resonances in a fiber under axial strain, to measure these coefficients [37]. This technique has the additional advantage that, since it does not involve the conventional modes of the fiber, there is no need that the FUTs are single mode in order to carry out the measurements. Then, the coefficients can be measured at different wavelengths to determine their dispersion; this is a limitation of the usual technique based on the optical activity which is overcome by means of WGM technique [38].

According to Eq. (1), a variation in the refractive index will tune the WGM resonances in wavelength. In this case, an axial strain will be applied to the FUT in order to induce this variation in the index, due to the elasto-optic effect. This feature was applied in different works in order to tune the WGM resonances

[39, 40]. However, there was not any mention to the different behaviors of TE- and TM-WGM.

An axial strain introduces a refractive index perturbation in an isotropic, cylindrical MR, due to the elasto-optic effect, which will be different for the axial (Δn_z) and transversal directions (Δn_t):

$$\frac{\Delta n_t}{n_0} = -p_{et}\varepsilon; \qquad p_{et} \equiv \frac{n_0^2}{2}\left(p_{12} - \nu(p_{11} + p_{12})\right), \tag{8}$$

$$\frac{\Delta n_z}{n_0} = -p_{ez}\varepsilon; \qquad p_{ez} \equiv \frac{n_0^2}{2}\left(p_{11} - 2\nu p_{12}\right), \tag{9}$$

where n_0 is the unperturbed index of the MR, p_{ij} are the elasto-optic coefficients, ν is Poisson's ratio, and ε is the strain applied to the MR. The coefficients p_{et} and p_{ez} are the effective elasto-optic coefficients, which are defined for simplicity. According to the reported values for the elasto-optic coefficients for fused silica ($p_{11} = 0.121, p_{12} = 0.27$ [41], $\nu = 0.17$ [42]), the ratio $\Delta n_t/\Delta n_z \approx 6.97$; hence, it is expected that the strain introduces a significant differential anisotropy. With this in mind, Maxwell's equations will be solved considering the uniaxial tensor given by Eq. (2). The solutions, as mentioned before, split in two families of WGM, the TE and TM modes, whose resonant frequencies will be obtained by solving Eqs. (3) and (4).

The refractive index perturbation is not the only factor to take into account when evaluating the wavelength shift of WGM resonances due to strain: the radius a of the MR also varies with it according to Poisson's ratio, $\Delta a/\mathrm{a} = -\nu\varepsilon$.

With all these ideas in mind, the relative shift of the WGM resonances, $\Delta\lambda_R/\lambda_R$, can be characterized as a function of the strain, for TE- and TM-WGMs. **Figure 10a** shows an example of the anisotropic behavior of TE- and TM-WGM. The strain applied to the MR was 330 $\mu\varepsilon$ for both polarizations, and the measured wavelength shift was different for each of them: 0.18 nm for TE-WGM and 0.11 nm for TM-WGM. $\Delta\lambda_R/\lambda_R$ was measured as a function of the strain in detail at 1531 nm, for both polarizations; the results are shown in **Figure 10b**. A linear trend in both cases can be observed: the slopes of the linear regressions that fit the experimental values are $s_{\mathrm{TE}} = -0.369 \pm 0.006\ \mu\varepsilon^{-1}$ for the TE- and $s_{\mathrm{TM}} = -0.201 \pm 0.004\ \mu\varepsilon^{-1}$ for the TM-WGM. The ratio $s_{\mathrm{TE}}/s_{\mathrm{TM}} = 1.84$ shows the anisotropy of the elasto-optic effect. From these values, it is possible to calculate the elasto-optic coefficients p_{ij} with its uncertainties (see [37] for a more detailed description of the procedure), by taking

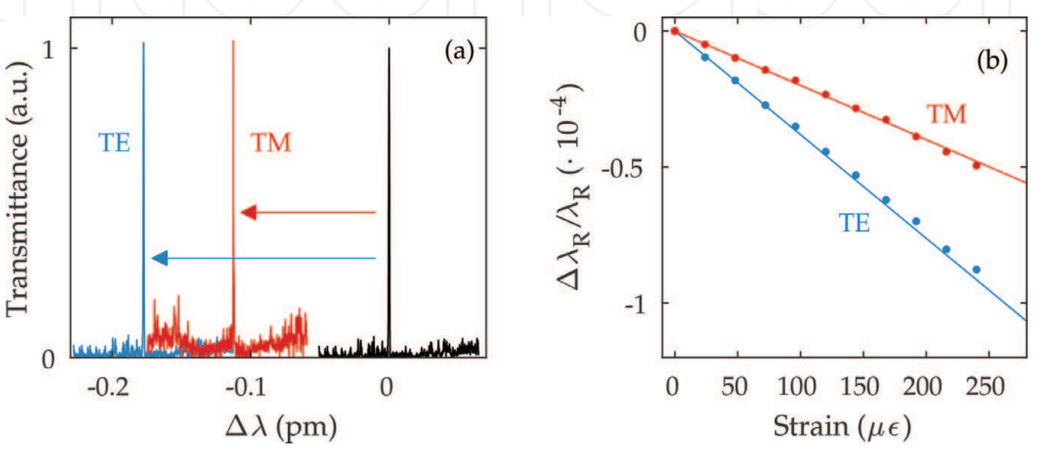

Figure 10.
(a) Wavelength shift of TE-/TM-WGM resonances for $\varepsilon = 330\ \mu\varepsilon$. (b) Measurement of the wavelength shift as a function of the strain.

	Present work		Literature
	1531 nm	**1064 nm**	
p_{11}	0.116	0.131	0.113 @ 633 nm [32]
			0.121 @ 633 nm [41]
p_{12}	0.255	0.267	0.252 @ 633 nm [32]
			0.270 @ 633 nm [41]

Table 3.
Comparison of experimental p_{ij} values with those reported in the literature.

into account the Sellmeier coefficients for the value of the refractive index at 1531 nm and Poisson's ratio of $\nu = 0.17 \pm 0.01$.

The measurements were repeated at 1064 nm, to study the dispersion of the elasto-optic effect. Results at both wavelengths are compiled in **Table 3** and are compared with those reported in the literature. Both sets of measurements are in good agreement, and the small differences might be due to the fact that the technique based in WGM measures the p_{ij} of the cladding material (i.e., fused silica), while in the case of the other techniques, the coefficients are determined by the material of the fiber core, which is usually silica doped with other elements.

7. Conclusions

In this chapter, we described a technique based on the excitation of WGMs around cylindrical MRs, to measure properties of the MR material. The resonant nature of the WGMs confers this technique with high sensitivity and low detection limits. Also, the technique allows measuring these parameters with axial resolution; hence, it is possible to detect changes of the parameters point to point along the MR.

The technique has been applied to different experiments. Mainly, thermo-optic effect and elasto-optic effect have been investigated in silica fibers. The variation in the index, due to a change in the temperature or strain, rules the shift in wavelength of the WGM resonances. When the technique was applied to different types of fibers and components, different information were obtained from the experiments. In particular, we measure temperature profiles in pumped, rare-earth doped fibers and in FBGs; the absorption coefficient in irradiated photosensitive fibers; and the Pockels coefficients in telecom fibers. Novel results were obtained: for example, it was possible to measure absorption and scattering loss coefficients separately, and, also, the anisotropy of the elasto-optic effect was observed experimentally. The information provided by the WGM-based technique might help to optimize the fabrication procedures of doped fibers and fiber components as FBGs or LPGs.

Acknowledgements

This work was funded by Ministerio de Economía y Competitividad of Spain and FEDER funds (Ref: TEC2016-76664-C2-1-R) and Generalitat Valenciana (Ref: PROMETEOII/2014/072), Universitat de València (UV-INV-AE16-485280). X. Roselló-Mechó's contract is funded by the FPI program (MinECo, Spain, BES-2014-068607). E. Rivera-Pérez's contract is funded by the Postdoctoral Stays in Foreigner Countries (291121, CONACYT, Mexico).

Author details

Martina Delgado-Pinar*, Xavier Roselló-Mechó, Emmanuel Rivera-Pérez, Antonio Díez, José Luis Cruz and Miguel V. Andrés
Applied Physics Department, Science Materials Institute, University of Valencia, Valencia, Spain

*Address all correspondence to: martina.delgado@uv.es

IntechOpen

References

[1] Rayleigh L. The Theory of Sound. Vol. 2. London: Macmillan; 1896

[2] Mie G. Beiträge zur Optik trüber Medien, speziell kolloidaler Metallösungen. Annalen der Physik. 1908;**330**(3):377-445. DOI: 10.1002/andp.19083300302

[3] Debye P. Der Lichtdruck auf Kugeln von beliebigem Material. Annalen der Physik. 1909;**335**(11):57-136. DOI: 10.1002/andp.19093351103

[4] Richtmyer RD. Dielectric resonators. Journal of Applied Physics. 1939;**10**(6): 391-398. DOI: 10.1063/1.1707320

[5] Stratton JA. Electromagnetic Theory. 1st ed. New York: McGraw-Hill; 1941

[6] Braginsky VB, Gorodetsky ML, Ilchenko VS. Quality-factor and nonlinear properties of optical whispering-gallery modes. Physics Letters A. 1989;**137**(7):393-397. DOI: 10.1016/0375-9601(89)90912-2

[7] Sumetsky M. Mode localization and the Q-factor of a cylindrical microresonator. Optics Letters. 2010; **35**(14):2385-2387. DOI: 10.1364/OL.35.002385

[8] Knight JC, Cheung G, Jacques F, Birks TA. Phase-matched excitation of whispering-gallery-mode resonances by a fiber taper. Optics Letters. 1997; **22**(15):1129-1131. DOI: 10.1364/OL.22.001129

[9] Gorodetsky ML, Savchenkov AA, Ilchenko VS. Ultimate Q of optical microsphere resonators. Optics Letters. 1996;**21**(7):453-455. DOI: 10.1364/OL.21.000453

[10] Armani DK, Kippenberg TJ, Spillane SM, Vahala KJ. Ultra-high-Q toroid microcavity on a chip. Nature. 2003; **421**:925-928. DOI: 10.1038/nature01371

[11] Roselló-Mechó X, Delgado-Pinar M, Cruz JL, Díez A, Andrés MV. Measurement of UV-induced absorption and scattering losses in photosensitive fibers. Optics Letters. 2018;**43**(12): 2897-2900. DOI: 10.1364/OL.43.002897

[12] Armani AM, Kulkarni RP, Fraser SE, Flagan RC, Vahala KJ. Label-free, single-molecule detection with optical microcavities. Science. 2007;**317**(5839): 783-787. DOI: 10.1126/science.1145002

[13] Birks TA, Knight JC, Dimmick TE. High-resolution measurement of the fiber diameter variations using whispering gallery modes and no optical alignment. IEEE Photonics Technology Letters. 2000;**12**(2):182-183. DOI: 10.1109/68.823510

[14] Rivera-Pérez E. Microcavidades ópticas cilíndricas y sus aplicaciones [thesis]. Universidad Autónoma de San Luis de Potosí-IICO; 2015. pp. 1-84

[15] Schiller S, Byer RL. High-resolution spectroscopy of whispering gallery modes in large dielectric spheres. Optics Letters. 1991;**16**(15):1138-1140. DOI: 10.1364/OL.16.001138

[16] Arques L, Carrascosa A, Zamora V, Díez A, Cruz JL, Andrés MV. Excitation and interrogation of whispering-gallery modes in optical microresonators using a single fused-tapered fiber tip. Optics Letters. 2011;**36**(17):3452-3454. DOI: 10.1364/OL.36.003452

[17] Kenny RP, Birks TA, Oakley KP. Control of optical fibre taper shape. Electronics Letters. 1991;**27**(18): 1654-1656. DOI: 10.1049/el:19911034

[18] Sumetsky M, Dulashko Y. Radius variation of optical fibers with angstrom

accuracy. Optics Letters. 2010;**35**(23): 4006-4008. DOI: 10.1364/OL.35.004006

[19] Guan G, Arnold S, Otugen V. Temperature measurements using a microoptical sensor based on whispering gallery modes. AIAA Journal. 2006;**44**(10):2385-2389. DOI: 10.2514/1.20910

[20] Ma Q, Rossmann T, Guo Z. Temperature sensitivity of silica micro-resonators. Journal of Physics D: Applied Physics. 2008;**41**(24):245111. DOI: 10.1088/0022-3727/41/24/245111

[21] Rivera-Pérez E, Villegas IL, D´ ıez A, Andrés MV, Cruz JL, Rodríguez-Cobos A. Measurement of pump-induced temperature increase in doped fibers using whispering-gallery modes. IEEE Photonics Technology Letters. 2013;**25**(24):2498-2500. DOI: 10.1109/LPT.2013.2288865

[22] Wang Y, Xu CQ, Hong P. Thermal effects in kilowatt fiber lasers. IEEE Photonics Technology Letters. 2004; **16**(1):63-65. DOI: 10.1109/LPT.2003.818913

[23] Hadeler O, Ibsen M, Zervas MN. Distributed-feedback fiber laser sensor for simultaneous strain and temperature measurements operating in the radio-frequency domain. Applied Optics. 2001;**40**(19):3169-3175. DOI: 10.1364/AO.40.003169

[24] MJF D. Rare-earth-doped fiber lasers and amplifiers, revised and expanded. In: Optical Science and Engineering. Boca Raton: Taylor & Francis; 2001

[25] Davis MK, Digonnet MJF, Pantell RH. Thermal effects in doped fibers. Journal of Light-Wave Technology. 1998;**16**(6):1013-1023. DOI: 10.1109/50.681458

[26] Delgado-Pinar M, Villegas IL, Díez A, Cruz JL, Andrés MV. Measurement of temperature profile induced by the optical signal in fiber Bragg gratings using whispering-gallery modes. Optics Letters. 2014;**39**(21):6277-6280. DOI: 10.1364/OL.39.006277

[27] Poumellec B, Guénot P, Riant I, Sansonetti P, Niay P, Bernage P, et al. UV induced densification during Bragg grating inscription in Ge: SiO2 preforms. Optical Materials. 1995;**4**(4):441-449. DOI: 10.1016/0925-3467(94)00114-6

[28] Canning J, Åslund M, Hu PF. Ultraviolet-induced absorption losses in hydrogen-loaded optical fibers and in presensitized optical fibers. Optics Letters. 2000;**25**(22):1621-1623. DOI: 10.1364/OL.25.001621

[29] Arigiris A, Konstantaki M, Ikiades A, Chronis D, Florias P, Kallimani K, et al. Fabrication of high-reflectivity superimposed multiple-fiber Bragg gratings with unequal wave-length spacing. Optics Letters. 2002;**27**(15): 1306-1308. DOI: 10.1364/OL.27.001306

[30] Gagné M, Loranger S, Lapointe J, Kashyap R. Fabrication of high quality, ultra-long fiber Bragg gratings: Up to 2 million periods in phase. Optics Express. 2014;**22**(1):387-398. DOI: 10.1364/OE.22.000387

[31] Lauzon J, Thibault S, Martin J, Ouellette F. Implementation and characterization of fiber Bragg gratings linearly chirped by a temperature gradient. Optics Letters. 1994;**19**(23): 2027-2029. DOI: 10.1364/OL.19.002027

[32] Bertholds A, Dandliker R. Determination of the individual strain-optic coefficients in single-mode optical fibres. Journal of Lightwave Technology. 1988;**6**(1):17-20. DOI: 10.1109/50.3956

[33] Dragic PD, Ballato J, Morris S, Hawkins T. Pockels' coefficients of alumina in aluminosilicate optical fiber. Journal of the Optical Society of

America B: Optical Physics. 2013;**30**(2): 244-250. DOI: 10.1364/JOSAB.30.000244

[34] Bertholds A, Dandliker R. Deformation of single-mode optical fibers under static longitudinal stress. Journal of Lightwave Technology. 1987; **5**(7):895-900. DOI: 10.1109/JLT.1987.1075583

[35] Skelton SE, Sergides M, Patel R, Karczewska E, Maragó OM, Jones PH. Evanescent wave optical trapping and transport of micro- and nanoparticles on tapered optical fibers. Journal of Quantitative Spectroscopy and Radiation Transfer. 2012;**113**(18): 2512-2520. DOI: 10.1016/j.jqsrt.2012.06.005

[36] Lægsgaard J. Theory of surface second-harmonic generation in silica nanowires. Journal of the Optical Society of America B: Optical Physics. 2010;**27**(7):1317-1324. DOI: 10.1364/JOSAB.27.001317

[37] Roselló-Mechó X, Delgado-Pinar M, Díez A, Andrés MV. Measurement of Pockels' coefficients and demonstration of the anisotropy of the elasto-optic effect in optical fibers under axial strain. Optics Letters. 2016;**41**(13):2934-2937. DOI: 10.1364/OL.41.002934

[38] Jülich F, Aulbach L, Wilfert A, Kratzer P, Kuttler R, Roths J. Gauge factors of fibre Bragg grating strain sensors in different types of optical fibres. Measurement Science and Technology. 2013;**24**(9):094007. DOI: 10.1088/0957-0233/24/9/094007

[39] Pöllinger M, O'Shea D, Warken F, Rauschenbeutel A. Ultrahigh-Q tunable whispering-gallery-mode microresonator. Physical Review Letters. 2009;**103**:053901. DOI: 10.1103/PhysRevLett.103.053901

[40] Linslal CL, Kailasnath M, Mathew S, Nideep TK, Radhakrishnan P, Nampoori VPN, et al. Tuning whispering gallery lasing modes from polymer fibers under tensile strain. Optics Letters. 2016;**41**(3):551-554. DOI: 10.1364/OL.41.000551

[41] Lide DR. CRC Handbook of Chemistry and Physics. 84th ed. Boca Raton: CRC Press; 2003

[42] Shackelford JF, Alexander W. CRC Materials Science and Engineering Handbook. 3rd ed. Boca Raton: CRC Press; 2001